2004

Computational Modeling of Softening in a Structural Phase Transformation

Pavel Bělík
Augsburg University, belik@augsburg.edu

Mithcell Luskin
University of Minnesota - Twin Cities

Multiscale Modeling & Simulation, 3:764–781, 2004.

COMPUTATIONAL MODELING OF SOFTENING IN A STRUCTURAL PHASE TRANSFORMATION

PAVEL BĚLÍK AND MITCHELL LUSKIN

Abstract. We develop a free energy density to model a structural first-order phase transformation from a high-temperature cubic phase to a low-temperature tetragonal phase. The free energy density models the softening of the elastic modulus controlling the low-energy path from the cubic to the tetragonal lattice, the loss of stability of the tetragonal phase at high temperatures and the loss of stability of the cubic phase at low temperatures, and the effect of compositional fluctuation on the transformation temperature.

Numerical experiments are given for the quasi-static cooling and heating of a single crystal thin film through the transformation. Tweed-like oscillations are obtained as precursors to the structural phase transformation.

1. Introduction

Martensitic crystals undergo a structural first-order phase transformation from a high-symmetry crystal structure to a low-symmetry crystal structure when cooled through the transformation. The volume fractions of the phases change continuously over a range of temperatures rather than transforming at a single temperature, and hysteresis is observed [31]. The nature of the phase transformation is dependent not only on the constituents of the martensitic crystal alloy, but also on the defects created by the processing.

The development of models to understand and predict this complex transformational behavior has been a great challenge to researchers during the past few decades [3, 4, 6, 21, 22, 24, 26, 27, 29, 31–34]. We develop a geometrically nonlinear free energy density that models the softening of the elastic modulus that determines the low energy path from the cubic to the tetragonal phase, the loss of stability of the tetragonal phase at high temperatures, the loss of stability of the cubic phase at low temperatures, and the effect of compositional fluctuation on the transformation temperature. Our free energy density generalizes the Landau-Ginzburg free energy density proposed in [20] by allowing the matching of the elastic moduli for both the cubic and the tetragonal phases.

In this paper, we further use our free energy density in a rigorously derived thin film model [7, 8] that includes transverse shear and normal compression to computationally model the structural phase transformation in single crystal film as it is quasi-statically cooled and then heated through the transformation. Tweed-like oscillations are obtained as precursors to the structural phase transformation, similar to the tweed-like oscillations obtained in [20] for a two dimensional model.

Date: April 9, 2005.

2000 *Mathematics Subject Classification.* 65C30, 65Z05, 74K35, 74N10, 74N15, 74S05.

Key words and phrases. phase transformation, martensite, austenite, softening, tweed, precursor.

This work was supported in part by NSF DMS-0074043 and DMS-0304326, by AFOSR F49620-98-1-0433, by and by the Minnesota Supercomputer Institute. This work was also supported in part by the Army High Performance Computing Research Center (AHPCRC) under the auspices of the Department of the Army, Army Research Laboratory (ARL) under Cooperative Agreement number DAAD19-01-2-0014. The contents of the work do not necessarily reflect the position or policy of the government, and no official endorsement should be inferred.

These tweed-like oscillations have been observed experimentally in Ni_2MnGa, as well as in other martensitic crystals [11].

2. The free energy density with compositional fluctuation

We propose a free energy density for martensitic crystals with compositional fluctuation and softening by using the framework of the geometrically nonlinear theory for martensitic crystals [3,4,26,27]. Our composition-dependent free energy density $\phi(F,\theta,c)$ will be a continuous function $\phi : \mathbb{R}^{3\times3}_+ \times (\theta_0,\theta_1) \times [0,1] \to \mathbb{R}$ representing the free energy per unit reference volume of the material as a function of the deformation gradient $F \in \mathbb{R}^{3\times3}_+$, the temperature $\theta \in (\theta_0,\theta_1)$, and a compositional order parameter $c \in [0,1]$. We note that the deformation gradient, F, in the domain of the free energy density $\phi(F,\theta,c)$ has been restricted to the subgroup of 3×3 matrices with positive determinant, denoted by $\mathbb{R}^{3\times3}_+$, since the admissible deformations will be restricted to orientation-preserving mappings [10, 18]. The transformation temperature, θ_T, can be expected to depend monotonically and continuously on the composition, c. Hence, it will be convenient to denote the energy density as a function of transformation temperature, θ_T, rather than composition, c; and we will use the notation $\phi = \phi(F,\theta,\theta_T)$ for $F \in \mathbb{R}^{3\times3}_+$ and $\theta,\ \theta_T \in (\theta_0,\theta_1)$. The domain of temperatures (θ_0,θ_1) is taken to be large enough to contain all temperatures of interest.

We assume that the free energy density, $\phi = \phi(F,\theta,\theta_T)$, is frame-indifferent and respects the material symmetry of the cubic (austenitic) crystalline lattice. The frame-indifference can be mathematically expressed by

$$\phi(RF,\theta,\theta_T) = \phi(F,\theta,\theta_T) \quad \text{for all } R \in \mathrm{SO}(3),\ F \in \mathbb{R}^{3\times3}_+, \text{ and } \theta,\theta_T \in (\theta_0,\theta_1), \tag{2.1}$$

where SO(3) denotes the group of proper rotations. The material symmetry can be expressed by

$$\phi(FQ,\theta,\theta_T) = \phi(F,\theta,\theta_T) \quad \text{for all } Q \in \mathcal{G},\ F \in \mathbb{R}^{3\times3}_+, \text{ and } \theta,\theta_T \in (\theta_0,\theta_1), \tag{2.2}$$

where $\mathcal{G} \subset \mathrm{SO}(3)$ is the symmetry group of the cubic crystalline lattice.

We now give the properties that the free energy density must satisfy to model the first-order structural phase transformation at the transformation temperature, θ_T. We shall assume that at fixed temperatures $\theta > \theta_T$ the free energy density, $\phi(F,\theta,\theta_T)$, as a function of the deformation gradient $F \in \mathbb{R}^{3\times3}_+$ is minimized on the group of proper rotations of the reference lattice, SO(3); and that for fixed temperatures $\theta < \theta_T$ the free energy density as a function of $F \in \mathbb{R}^{3\times3}_+$ is minimized on

$$\mathcal{M} = \mathrm{SO}(3)U_1 \cup \cdots \cup \mathrm{SO}(3)U_N,$$

where for the symmetry group of the cubic phase, $\mathcal{G}$, we have that the transformation stretch matrices $\{U_1,\ldots,U_N\}$ for the tetragonal variants are given by

$$\{U_1,\ldots,U_N\} = \{Q^TU_1Q :\ Q \in \mathcal{G}\}.$$

When $\theta = \theta_T$, the free energy density is minimized at both the cubic phase ($F \in \mathrm{SO}(3)$) and the tetragonal phase ($F \in \mathcal{M}$) deformation gradients. Near the transformation temperature, both phases remain local minimizers of ϕ. We can summarize these exchange of stability properties by

$$\begin{aligned}
&\phi(R,\theta,\theta_T) < \phi(F,\theta,\theta_T), && F \in \mathbb{R}^{3\times3}_+ \setminus \mathrm{SO}(3), && \theta > \theta_T,\\
&\phi(R,\theta,\theta_T) = \phi(M,\theta,\theta_T) < \phi(F,\theta,\theta_T), && F \in \mathbb{R}^{3\times3}_+ \setminus \{\mathrm{SO}(3) \cup \mathcal{M}\}, && \theta = \theta_T,\\
&\phi(M,\theta,\theta_T) < \phi(F,\theta,\theta_T), && F \in \mathbb{R}^{3\times3}_+ \setminus \mathcal{M}, && \theta < \theta_T,
\end{aligned} \tag{2.3}$$

for $R \in \mathrm{SO}(3),\ M \in \mathcal{M}$. We note that the above assumptions neglect the dependence on temperature of the lattice constants for the cubic and tetragonal phases.

We shall now restrict our consideration in this paper to the cubic-to-tetragonal ($N = 3$) phase transformation. The high-temperature cubic phase is characterized by a single lattice constant, a_0, which is the length of a side of its cubic unit cell with volume equal to a_0^3. The low-temperature tetragonal phase is characterized by two lattice constants, a and c, which give the lengths of the sides of the transformed tetragonal unit cell with volume equal to $a^2 \cdot c$.

We shall identify the reference orthonormal coordinate system with the lattice axes of the cubic phase. With respect to this coordinate system, there are three transformation stretch matrices, U_1, U_2, and U_3, corresponding to the transformations of the cubic lattice to the lattice of the three tetragonal variants,

$$U_1 = \begin{pmatrix} \gamma & 0 & 0 \\ 0 & \alpha & 0 \\ 0 & 0 & \alpha \end{pmatrix}, \qquad U_2 = \begin{pmatrix} \alpha & 0 & 0 \\ 0 & \gamma & 0 \\ 0 & 0 & \alpha \end{pmatrix}, \qquad U_3 = \begin{pmatrix} \alpha & 0 & 0 \\ 0 & \alpha & 0 \\ 0 & 0 & \gamma \end{pmatrix}, \tag{2.4}$$

where the transformation stretches are given by

$$\alpha = \frac{a}{a_0} \qquad \text{and} \qquad \gamma = \frac{c}{a_0}. \tag{2.5}$$

We will construct in Section 3 a free energy density for the cubic phase, $W_A(C, \theta)$, and in Section 4 we will construct a free energy density for the tetragonal phase, $W_M(C, \theta)$, such that the free energy densities are functions of the right Cauchy-Green strain, $C = F^T F$, to guarantee that the frame-indifference property (2.1) holds [10,18]. The free energy densities that we will construct will also satisfy the material symmetry property (2.2) expressed in terms of the right Cauchy-Green strain, that is,

$$\begin{aligned} W_A(Q^T C Q, \theta) &= W_A(C, \theta) \quad \text{for all } Q \in \mathcal{G},\ C \in \mathbb{S}^{3\times 3}_+, \text{ and } \theta \in (\theta_0, \theta_1), \\ W_M(Q^T C Q, \theta) &= W_M(C, \theta) \quad \text{for all } Q \in \mathcal{G},\ C \in \mathbb{S}^{3\times 3}_+, \text{ and } \theta \in (\theta_0, \theta_1), \end{aligned} \tag{2.6}$$

where $\mathbb{S}^{3\times 3}_+$ denotes the group of 3×3 symmetric, positive definite matrices.

The cubic and tetragonal free energy densities will be normalized to be nonnegative and to be zero only at their respective energy wells, so that for $\theta > M_s$ where $M_s < \theta_T$ is the temperature at which the cubic phase "softens" (see Section 3)

$$W_A(F^T F, \theta) = 0 \quad \text{if and only if} \quad F \in \mathrm{SO}(3), \tag{2.7}$$

and for $\theta \in (\theta_0, \theta_1)$

$$W_M(F^T F, \theta) = 0 \quad \text{if and only if} \quad F \in \mathcal{M} = \mathrm{SO}(3)U_1 \cup \mathrm{SO}(3)U_2 \cup \mathrm{SO}(3)U_3. \tag{2.8}$$

The energy densities $W_A(C, \theta)$ and $W_M(C, \theta)$ are also constructed to approximately match the elastic moduli at their respective energy wells.

The free energy density $\phi(F, \theta, \theta_T)$ is then defined in terms of the right Cauchy-Green strain, $C = F^T F$, to be

$$\phi(F, \theta, \theta_T) = \min\{W_A(C, \theta),\ W_M(C, \theta) + \eta(\theta, \theta_T)\}, \tag{2.9}$$

where for A_f and M_f satisfying $\theta_0 < M_f < M_s < \theta_T < A_f < \theta_1$, the free energy difference between the cubic and tetragonal phases, $\eta(\theta, \theta_T)$, satisfies

$$\eta(\theta, \theta_T) = \begin{cases} W_A(U_1^2, A_f)\, \frac{\theta - \theta_T}{A_f - \theta_T} & \text{for } \theta_T \le \theta < \theta_1, \\ -W_M(I, M_f)\, \frac{\theta - \theta_T}{M_f - \theta_T} & \text{for } \theta_0 < \theta < \theta_T. \end{cases} \tag{2.10}$$

The free energy difference between the cubic and tetragonal phases, $\eta(\theta, \theta_T)$, was constructed to be the piecewise linear function with the property that the local minimum corresponding to the tetragonal phase ($F \in \mathcal{M}$) disappears at $\theta = A_f$, and the local minimum corresponding to the

cubic phase ($F \in \mathrm{SO}(3)$) disappears at $\theta = M_f$. At $\theta = \theta_T$, the free energy density for both the cubic phase ($F \in \mathrm{SO}(3)$) and the tetragonal phase ($F \in \mathcal{M}$) are equal to zero, and the free energy difference $\eta(\theta_T, \theta_T)$ is equal to zero.

Since the cubic and tetragonal free energy densities, $W_A(C, \theta)$ and $W_M(C, \theta)$, are functions of the right Cauchy-Green strain, $C = F^T F$, we can immediately conclude from (2.9) that the free energy density $\phi(F, \theta, \theta_T)$ satisfies the frame-indifference property (2.1). Likewise, since the austentic and martensitic free energy densities satisfy the material symmetry property (2.6) for the cubic symmetry group, $\mathcal{G}$, we can conclude from (2.9) that the free energy density $\phi(F, \theta, \theta_T)$ satisfies the material symmetry property (2.2) for the cubic symmetry group, $\mathcal{G}$. Finally, it follows from (2.7), (2.8), (2.9), and (2.10) that the free energy density $\phi(F, \theta, \theta_T)$ satisfies the exchange of stability property (2.3).

The temperature M_s is usually identified experimentally with the temperature at which martensite first appears during cooling, and the temperature M_f is identified experimentally with the temperature at which the crystal has completely transformed to martensite [31]. Similarly, the temperature A_f is identified experimentally with the temperature at which the crystal has completely transformed to austenite during heating. The transformation temperature θ_T can then be determined, for example, from $\theta_T = (M_s + A_f)/2$ as proposed in [31].

The compositional fluctuation in a crystal alloy depends on the conditions of its growth. The temperatures M_f, M_s, θ_T, A_f introduced above are assumed to be defined as functions of a composition computed by averaging on a length scale that is small with respect to the length scale of the crystal. We can then consider M_f, M_s, θ_T, A_f to be functions of a spatially varying composition (see Section 7).

In the following sections, we shall derive a mathematical model for the energy density, the compositional fluctuation, and the thin film approximation. Our goal is to investigate the qualitative features of this model, and we attempt to model the the moduli and parameters from experimental data when available.

3. The austenitic (cubic) free energy density, $W_A(C, \theta)$, with softening

To construct $W_A(C, \theta)$, we first review some concepts from linear and finite elasticity [10, 18]. If $u : \Omega \to \mathbb{R}^3$ denotes the deformation of the crystal respect to its reference configuration Ω, then the displacement $v : \Omega \to \mathbb{R}^3$ is defined by $v(x) = u(x) - x$. We can then define the linear strain matrix $E : \Omega \to \mathbb{S}^{3\times 3}$ by

$$E(x) = \tfrac{1}{2}\left[\nabla v(x) + (\nabla v(x))^T\right]$$

and the finite strain $\mathfrak{E} : \Omega \to \mathbb{S}^{3\times 3}$ by

$$\begin{aligned}\mathfrak{E}(x) &= \tfrac{1}{2}\left[\nabla v(x) + (\nabla v(x))^T + (\nabla v(x))^T(\nabla v(x))\right] \\ &= E(x) + \tfrac{1}{2}(\nabla v(x))^T(\nabla v(x)).\end{aligned}$$

For the right Cauchy-Green strain, $C : \Omega \to \mathbb{S}^{3\times 3}_+$, we can check that

$$C(x) = (\nabla u(x))^T(\nabla u(x)) = I + 2\mathfrak{E}(x) = I + 2E + (\nabla v(x))^T(\nabla v(x)).$$

The general free energy density with cubic symmetry and quadratic in the strain matrix elements $E_{ij} \in \mathbb{R}$ of the linear strain matrix $E \in \mathbb{S}^{3\times 3}$ is given by [25]

$$\begin{aligned}\tilde{W}_A(E,\theta) &= \tfrac{1}{2}\mathbb{C}_{11}^A \left(E_{11}^2 + E_{22}^2 + E_{33}^2\right) + \mathbb{C}_{12}^A \left(E_{11}E_{22} + E_{11}E_{33} + E_{22}E_{33}\right) \\ &\qquad + 2\,\mathbb{C}_{44}^A \left(E_{12}^2 + E_{23}^2 + E_{13}^2\right) \\ &= \tfrac{1}{6}(\mathbb{C}_{11}^A - \mathbb{C}_{12}^A)\left[(E_{11}-E_{22})^2 + (E_{22}-E_{33})^2 + (E_{11}-E_{33})^2\right] \\ &\qquad + \tfrac{1}{6}(\mathbb{C}_{11}^A + 2\,\mathbb{C}_{12}^A)\left(E_{11}+E_{22}+E_{33}\right)^2 + 2\,\mathbb{C}_{44}^A \left(E_{12}^2 + E_{23}^2 + E_{13}^2\right),\end{aligned} \tag{3.1}$$

where the cubic elastic moduli $\mathbb{C}_{11}^A$, $\mathbb{C}_{12}^A$, and $\mathbb{C}_{44}^A$ depend on the temperature θ and can be determined experimentally. We note that Love [25] gives quadratic elastic energies in the variables

$$e_{xx} = E_{11}, \quad e_{yy} = E_{22}, \quad e_{zz} = E_{33}, \quad e_{xy} = 2E_{12}, \quad e_{yz} = 2E_{23}, \quad e_{zx} = 2E_{13}.$$

Neglecting the higher-order terms in the difference $\mathfrak{E} - E$, we substitute $\frac{1}{2}(C - I)$ for E to get

$$\begin{aligned}W_A(C,\theta) &= \tfrac{1}{24}(\mathbb{C}_{11}^A - \mathbb{C}_{12}^A)\left[(C_{11}-C_{22})^2 + (C_{22}-C_{33})^2 + (C_{11}-C_{33})^2\right] \\ &\qquad + \tfrac{1}{24}(\mathbb{C}_{11}^A + 2\,\mathbb{C}_{12}^A)\left(\operatorname{tr} C - 3\right)^2 + \tfrac{1}{2}\mathbb{C}_{44}^A \left(C_{12}^2 + C_{23}^2 + C_{13}^2\right)\end{aligned}$$

where $C_{ij} \in \mathbb{R}$ are the matrix elements of the right Cauchy-Green strain $C \in \mathbb{S}^{3\times 3}$. We introduce the following linear combinations of the elastic moduli $\mathbb{C}_{11}^A$, $\mathbb{C}_{12}^A$, and $\mathbb{C}_{44}^A$

$$a(\theta) = \tfrac{1}{24}(\mathbb{C}_{11}^A - \mathbb{C}_{12}^A), \qquad b(\theta) = \tfrac{1}{24}(\mathbb{C}_{11}^A + 2\,\mathbb{C}_{12}^A), \qquad c(\theta) = \tfrac{1}{2}\mathbb{C}_{44}^A,$$

and rewrite the above energy in terms of the matrix elements $C_{ij} \in \mathbb{R}$ of the right Cauchy-Green strain $C \in \mathbb{S}^{3\times 3}$ by

$$\begin{aligned}W_A(C,\theta) &= a(\theta)\left[(C_{11}-C_{22})^2 + (C_{22}-C_{33})^2 + (C_{11}-C_{33})^2\right] \\ &\qquad + b(\theta)\left(\operatorname{tr} C - 3\right)^2 + c(\theta)\left(C_{12}^2 + C_{23}^2 + C_{13}^2\right).\end{aligned} \tag{3.2}$$

It is observed in many martensitic alloys that the modulus $a(\theta) = \frac{1}{24}(\mathbb{C}_{11}^A - \mathbb{C}_{12}^A) = \frac{1}{12}\mathbb{C}'$ decreases to almost 0 (or is said to "soften" [20]) as the temperature decreases to the transformation temperature. The other two moduli, $b(\theta)$ and $c(\theta)$, typically exhibit weaker temperature dependence.

Experimental data [28] for the temperature dependence of the elastic moduli for $Fe_{70}Pd_{30}$ show that during cooling the tetragonal phase starts to appear at $M_s = 265$ K. Measured values of the elastic moduli are given for $\mathbb{C}_L^A = (\mathbb{C}_{11}^A + \mathbb{C}_{12}^A + 2\mathbb{C}_{44}^A)/2$ and $\mathbb{C}_{44}^A$ over a temperature range from about 220 K to about 430 K, and for $\mathbb{C}' = (\mathbb{C}_{11}^A - \mathbb{C}_{12}^A)/2 = 12a$ over a range from about 290 K to about 430 K. We fit this data for the elastic moduli by the linear approximation

$$a(\theta) \approx 0.0185\,\tilde{\theta} \text{ GPa}, \qquad b(\theta) \approx \left(17.2 - 0.0196\,\tilde{\theta}\right) \text{ GPa}, \qquad c(\theta) \approx \left(36.3 + 0.005\,\tilde{\theta}\right) \text{ GPa},$$

where

$$\tilde{\theta} = \max\{\theta - M_s, 0\}.$$

We notice that even though the measurement of $\mathbb{C}'(\theta) = 12a(\theta)$ is missing below 290 K, we allow the full softening of $a(\theta)$ to 0. This appears to be supported by the linear behavior of the measured $\mathbb{C}'$, which, if extrapolated below 290 K appears to vanish at $M_s = 265$ K. Notice that the above choice of $a(\theta)$, $b(\theta)$, and $c(\theta)$ makes $W_A(C,\theta)$ positive definite for $\theta > M_s$ and positive semidefinite for $\theta \le M_s$. Due to the construction of $\phi(F,\theta,\theta_T)$ as a minimum of $W_A(C,\theta)$ and $W_M(C,\theta) + \eta(\theta,\theta_T)$, we do not want to allow $W_A(C,\theta)$ to become indefinite.

4. The martensitic (tetragonal) free energy density, $W_M(C,\theta)$

We now discuss the construction of the martensitic part of the free energy density, $W_M(C,\theta)$. Similar to the construction of $W_A(C,\theta)$, we start from the quadratic elastic energy density with tetragonal symmetry in terms of the linear strain [25]. The situation is different here, though, because the reference configuration for this quadratic energy is the tetragonal lattice characterized by the stretch U_3 in our reference configuration (we could also have chosen to use the stretches U_1 or U_2). In particular, this change of coordinate system can be expressed by

$$F = \tilde{F}U_3,$$

where F is the deformation gradient in the reference coordinate of the cubic system and $\tilde{F}$ is the deformation gradient in the tetragonal coordinate system. We shall use the tilde symbol $\tilde{}$ to distinguish the quantities in the tetragonal coordinate system from their counterparts in the cubic reference system. In this way, we can define the quadratic free energy density with tetragonal symmetry $\tilde{W}_{M_3}(\tilde{E},\theta)$ near U_3 by starting from Love's expression [25]

$$\begin{aligned}\tilde{W}_{M_3}(\tilde{E},\theta) &= \tfrac{1}{2}\mathbb{C}^M_{11}(\tilde{E}^2_{11}+\tilde{E}^2_{22}) + \tfrac{1}{2}\mathbb{C}^M_{33}\tilde{E}^2_{33} + \mathbb{C}^M_{12}\tilde{E}_{11}\tilde{E}_{22}\\ &\quad + \mathbb{C}^M_{13}\tilde{E}_{33}(\tilde{E}_{11}+\tilde{E}_{22}) + 2\,\mathbb{C}^M_{44}(\tilde{E}^2_{23}+\tilde{E}^2_{13}) + 2\,\mathbb{C}^M_{66}\tilde{E}^2_{12}\\ &= \tfrac{1}{4}(\mathbb{C}^M_{11}-\mathbb{C}^M_{12})(\tilde{E}_{11}-\tilde{E}_{22})^2 + \tfrac{1}{4}(\mathbb{C}^M_{11}+\mathbb{C}^M_{12})(\tilde{E}_{11}+\tilde{E}_{22})^2\\ &\quad + \mathbb{C}^M_{13}\tilde{E}_{33}(\tilde{E}_{11}+\tilde{E}_{22}) + \tfrac{1}{2}\mathbb{C}^M_{33}\tilde{E}^2_{33} + 2\,\mathbb{C}^M_{44}(\tilde{E}^2_{23}+\tilde{E}^2_{13}) + 2\,\mathbb{C}^M_{66}\tilde{E}^2_{12}.\end{aligned}$$

It is now easy to see that the eigenvalues of the quadratic form $\tilde{W}_{M_3}(\tilde{E},\theta)$ are $\mathbb{C}^M_{44}$ (with multiplicity two), $\mathbb{C}^M_{66}$, and the three eigenvalues of the matrix

$$\begin{bmatrix}\mathbb{C}^M_{11} & \mathbb{C}^M_{12} & \mathbb{C}^M_{13}\\ \mathbb{C}^M_{12} & \mathbb{C}^M_{11} & \mathbb{C}^M_{13}\\ \mathbb{C}^M_{13} & \mathbb{C}^M_{13} & \mathbb{C}^M_{33}\end{bmatrix}, \tag{4.1}$$

which are

$$\mathbb{C}^M_{11}-\mathbb{C}^M_{12} \qquad \text{and} \qquad \tfrac{1}{2}\left[\mathbb{C}^M_{11}+\mathbb{C}^M_{12}+\mathbb{C}^M_{33} \pm \sqrt{\left(\mathbb{C}^M_{11}+\mathbb{C}^M_{12}-\mathbb{C}^M_{33}\right)^2 + 8\,\left(\mathbb{C}^M_{13}\right)^2}\right]. \tag{4.2}$$

The eigenvalue $\mathbb{C}^M_{11}-\mathbb{C}^M_{12}$ vanishes when $\mathbb{C}^M_{12}=\mathbb{C}^M_{11}$, and the smaller of the other eigenvalues in (4.2) vanishes when

$$\left(\mathbb{C}^M_{13}\right)^2 = \tfrac{1}{2}(\mathbb{C}^M_{11}+\mathbb{C}^M_{12})\,\mathbb{C}^M_{33}.$$

Thus, we see that our model can also treat softening in the tetragonal phase, but in this paper we will only consider tetragonal elastic moduli for which the quadratic form $\tilde{W}_{M_3}(E,\theta)$ always remains positive definite.

Proceeding now as in the definition of $W_A(C,\theta)$, we shall replace the linear strain $\tilde{E}$ in $\tilde{W}_{M_3}(\tilde{E},\theta)$ by the finite strain $\tilde{\mathfrak{E}} = \frac{1}{2}(\tilde{C}-I)$ where $\tilde{C}=\tilde{F}^T\tilde{F}$. Since $F=\tilde{F}U_3$ and U_3 is symmetric, we have that $\tilde{C}=U_3^{-1}CU_3^{-1}$, and therefore $\tilde{E}$ shall be replaced by the finite strain

$$\tilde{\mathfrak{E}} = \tfrac{1}{2}U_3^{-1}CU_3^2U_3^{-1} - I.$$

The free energy density $W_{M_3}(C,\theta)$ as a function of C then becomes

$$\begin{aligned}W_{M_3}(C,\theta) &= d\left[(C_{11}-\alpha^2)^2+(C_{22}-\alpha^2)^2\right] + e(C_{33}-\gamma^2)^2 + f(C_{11}-\alpha^2)(C_{22}-\alpha^2)\\ &\quad + g(C_{33}-\gamma^2)(C_{11}+C_{22}-2\alpha^2) + h_1(C^2_{23}+C^2_{13}) + h_2C^2_{12},\end{aligned}$$

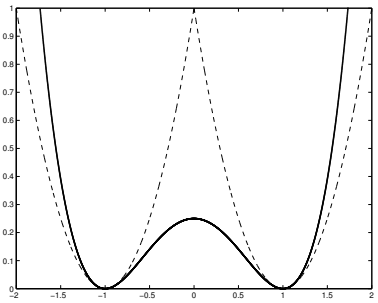

FIGURE 1. Comparison of $\min\{(x-1)^2,(x+1)^2\}$ (dashed line) and $\frac{1}{4}(x-1)^2(x+1)^2$ (thick line). Both functions have the same minima and the same second derivatives at ± 1; however, the barrier height at $x=0$ is 1 and $\frac{1}{4}$, respectively.

where

$$d = \mathbb{C}_{11}^M/8\alpha^4, \qquad e = \mathbb{C}_{33}^M/8\gamma^4, \qquad f = \mathbb{C}_{12}^M/4\alpha^4,$$
$$g = \mathbb{C}_{13}^M/4(\alpha\gamma)^2, \qquad h_1 = \mathbb{C}_{44}^M/2(\alpha\gamma)^2, \qquad h_2 = \mathbb{C}_{66}^M/2\alpha^4.$$

The free energy densities $W_{M_1}(C,\theta)$ and $W_{M_2}(C,\theta)$, minimized at U_1^2 and U_2^2, respectively, are then constructed by symmetry from

$$W_{M_1}(C,\theta) = W_{M_3}\left(R\left(\frac{\pi}{2}, e_2\right)^T CR\left(\frac{\pi}{2}, e_2\right), \theta\right) \qquad \text{for all } C \in \mathbb{S}_+^{3\times 3},$$
$$W_{M_2}(C,\theta) = W_{M_3}\left(R\left(\frac{\pi}{2}, e_1\right)^T CR\left(\frac{\pi}{2}, e_1\right), \theta\right) \qquad \text{for all } C \in \mathbb{S}_+^{3\times 3},$$

where $R\left(\frac{\pi}{2}, e_i\right) \in \mathcal{G}$ denotes the rotation of $\frac{\pi}{2}$ radians about the orthogonal basis vectors $e_i \in \mathbb{R}^3$.

We could construct the martensitic free energy density $W_M(C,\theta)$ as the minimum of the energy densities $W_{M_i}(C,\theta)$ by

$$W_M(C,\theta) = \min_{1\le i\le 3} W_{M_i}(C,\theta).$$

However, this would result in large energy barriers between the energy wells of the tetragonal variants U_i^2. To develop a martensitic free energy density $W_M(C,\theta)$ with the same elastic moduli at the energy wells U_i^2, but with lower energy barriers, we consider two one-dimensional models. The function $\frac{1}{4}(x-1)^2(x+1)^2$ has the same minima and the same second derivatives at ± 1 as the function $\min\{(x-1)^2,(x+1)^2\}$ (see Fig. 1). However, we note that the difference in the size of the energy barrier at $x=0$ quadruples if the minimum function is used. Further research is needed to clarify the effect of the magnitude of the energy barriers used in models for martensitic phase transitions and to determine how to calibrate the magnitude of the energy barriers by experimental results [1].

We now note that by construction of the free energy densities $W_{M_i}(C,\theta)$, there exists $\nu > 0$ independent of i and j, such that

$$W_{M_i}(U_j^2,\theta) = \nu \qquad \text{for } i \ne j.$$

It then follows that the quartic function

$$W_M^i(C,\theta) = \frac{1}{2\nu} W_{M_i}(C,\theta) \sum_{j=1}^{3} \left[W_{M_j}(C,\theta)(1-\delta_{ij})\right]$$

is nonnegative, equals 0 only at the variants U_i^2, and has the prescribed tetragonal elastic moduli $\mathbb{C}$ at U_i^2. Finally, we define $W_M(C,\theta)$ by

$$W_M(C,\theta) = \min_{1\le i\le 3} W_M^i(C,\theta).$$

We will present numerical results for the following two qualitatively different sets of elastic moduli (in GPa) for the martensitic free energy density $W_M(C,\theta)$

$$\mathbb{C}_{11}^M = 170, \quad \mathbb{C}_{33}^M = 110, \quad \mathbb{C}_{12}^M = 160, \quad \mathbb{C}_{13}^M = 118, \quad \mathbb{C}_{44}^M = 70, \quad \mathbb{C}_{66}^M = 75; \tag{4.3}$$

$$\mathbb{C}_{11}^M = 130, \quad \mathbb{C}_{33}^M = 190, \quad \mathbb{C}_{12}^M = 120, \quad \mathbb{C}_{13}^M = 140, \quad \mathbb{C}_{44}^M = 70, \quad \mathbb{C}_{66}^M = 75. \tag{4.4}$$

The major quantitative difference in the elastic moduli (4.3) and (4.4) is the relative magnitude of $\mathbb{C}_{11}^M$ and $\mathbb{C}_{33}^M$— in the first set $\mathbb{C}_{11}^M > \mathbb{C}_{33}^M$ and in the second set $\mathbb{C}_{11}^M < \mathbb{C}_{33}^M$. The common feature of these two sets of moduli are that the corresponding eigenvalues (4.2) of the matrix (4.1) are exactly 10, approximately 20, and approximately 420.

Since we did not have measured values of the elastic moduli for the martensitic phase of $Fe_{70}Pd_{30}$, we were motivated by the analysis in [13,14] to choose the eigenvalue $\mathbb{C}_{11}^M - \mathbb{C}_{12}^M$ and the smaller of the pair of eigenvalues in (4.2) to be small and the larger eigenvalue of the pair in (4.2) to be relatively large. We chose the approximate values 10 and 20 for the eigenvalue $\mathbb{C}_{11}^M - \mathbb{C}_{12}^M$ and the smaller of the pair of eigenvalues in (4.2). We chose the larger root in (4.2) so that the sum of the eigenvalues of the matrix (4.1) is 450 to approximately equal the sum of the corresponding eigenvalues for the cubic phase (which is equal to $3\mathbb{C}_{11}^A$ by (3.1)) above the transformation temperature.

We were also motivated by the analysis in [13,14] to choose the martensitic moduli $\mathbb{C}_{44}^M$ and $\mathbb{C}_{66}^M$ close to the austenitic modulus $\mathbb{C}_{44}^A$ and by the analysis in [9] to choose $\mathbb{C}_{66}^M > \mathbb{C}_{44}^M$. We have chosen the values $\mathbb{C}_{66}^M = 75$ GPa and $\mathbb{C}_{44}^M = 70$ GPa since the austenitic modulus $\mathbb{C}_{44}^A$ approaches 72.65 GPa as θ approaches M_s.

5. The sharp interface thin film model and its finite element approximation

We have rigorously derived a sharp interface thin film free energy [8] from a bulk free energy in which interfacial energy was modeled by the total variation of the deformation gradient following earlier work on a diffuse interface model [5]. We consider a film of thickness $h > 0$ with reference state $\Omega_h \equiv \mathcal{S} \times (-h/2,\, h/2)$ where $\mathcal{S} \subset \mathbb{R}^2$ is a domain with a Lipschitz continuous boundary $\partial\mathcal{S}$. Since the composition varies in the crystal, the transformation temperature is given by $\theta_T : \Omega_h \to \mathbb{R}$. The bulk elastic free energy for the crystal with deformation $u : \Omega_h \to \mathbb{R}^3$ and temperature field $\theta : \Omega_h \to \mathbb{R}$ is then given by

$$\int_{\Omega_h} \phi(\nabla u(x), \theta(x), \theta_T(x))\, dx.$$

We model the interfacial energy in the thin layers separating regions between phases and variants by the product of a material constant, κ, and the surface areas of the interfaces. This interfacial energy model is described mathematically by

$$\kappa \int_{\Omega_h} |D(\nabla u)|,$$

where $\int_{\Omega_h} |D(\nabla u)|$ is the total variation of the deformation gradient [7, 8, 15, 17] defined by

$$\int_{\Omega} |D(\nabla u)|$$

$$= \sup \left\{ \sum_{i,j,k=1,2,3} \int_\Omega u_{i,j}(x)\psi_{ijk,k}(x)\,dx : \psi \in \mathcal{C}_0^\infty(\Omega;\mathbb{R}^{3\times 3\times 3}),\ |\psi(x)| \le 1 \text{ for all } x \in \Omega \right\}$$

The vector norm $|\cdot|$ above is the usual euclidean norm, that is, the square root of the sum of the squares of all the components. The total variation of a deformation gradient ∇u that is discontinuous across the piecewise smooth surfaces $\sigma_j,\ j = 1, \dots, J$, separating the open sets ω_ℓ in the disjoint union $\Omega_h = \sum_{\ell=1}^L \omega_\ell$ is given by

$$\int_{\Omega_h} |D(\nabla u)| = \sum_{j=1}^J \int_{\sigma_j} |[\![\, \nabla u \,]\!]_{\sigma_j}|\,dS + \sum_{\ell=1}^L \int_{\omega_\ell} \sqrt{\sum_{m,n=1}^3 \left(\frac{\partial^2 u}{\partial x_m \partial x_n}\right)^2}\,dx$$

where $[\![\, \nabla u \,]\!]_{\sigma_j}$ denotes the jump of the deformation gradient across the interface σ_j. The total energy for the film is then given by the following sum of the interfacial energy and the elastic energy

$$\kappa \int_{\Omega_h} |D(\nabla u)| + \int_{\Omega_h} \phi(\nabla u(x), \theta(x), \theta_T(x))\,dx. \tag{5.1}$$

Our analysis of the thin film limit $h \to 0$ of the bulk energy (5.1) assumed that the energy density $\phi(F, \theta, \theta_T)$ satisfied the growth condition

$$c_1(|F|^p - 1) \le \phi(F, \theta, \theta_T) \le c_2(|F|^p + 1) \quad \text{for all } F \in \mathbb{R}^{3\times 3}_+ \text{ and } \theta, \theta_T \in (\theta_0, \theta_1), \tag{5.2}$$

where c_1 and c_2 are fixed positive constants and $p > 3$ to ensure that deformations with finite energy are uniformly continuous [2,16]. We showed (for the case that the deformations are constrained on the lateral boundary $\partial\mathcal{S} \times (-h/2,\ h/2)$ and the temperature fields θ and θ_T do not vary in space) that the minimum energy of (5.1) can be approximated for $h \to 0$ by the energy of

$$u(x_1, x_2, x_3) = y(\tilde{x}) + b_\varepsilon(\tilde{x})x_3 \quad \text{for } \tilde{x} = (x_1, x_2) \in \mathcal{S},\ x_3 \in (-h/2,\ h/2), \tag{5.3}$$

for $b_\varepsilon \in W^{1,p}(\mathcal{S})$ a smooth approximation of b where $(y, b) : \mathcal{S} \to \mathbb{R}^3 \times \mathbb{R}^3$ minimizes the thin film energy

$$\mathcal{E}(y, b; \theta, \theta_T) = \kappa \int_{\mathcal{S}} |D(\nabla y|\sqrt{2}b)| + \int_{\mathcal{S}} \phi(\nabla y(\tilde{x})|b(\tilde{x}), \theta(\tilde{x}), \theta_T(\tilde{x}))\,d\tilde{x} \tag{5.4}$$

over all pairs $(\tilde{y}, \tilde{b}) \in \mathcal{A}$, where the space of admissible deformations of the thin film is given by

$$\mathcal{A} = \{(\tilde{y}, \tilde{b}) \in W^{1,p}(\mathcal{S};\mathbb{R}^3) \times L^p(\mathcal{S};\mathbb{R}^3) :\ \nabla\tilde{y}, \tilde{b} \in BV(\mathcal{S})\}.$$

See [8] for the precise statement and analysis of the thin film approximation.

We can see by (5.3) that the map $y : \mathcal{S} \to \mathbb{R}^3$ describes the deformation of the midplane of the film, and the map $b : \mathcal{S} \to \mathbb{R}^3$ describes the deformation of the cross-section relative to the film [5, 7, 8]. We denote by $(\nabla y|b) \in \mathbb{R}^{3\times 3}$ the matrix whose first two columns are given by the columns of ∇y and the last column by b and occasionally refer to it as the "deformation gradient." The integral $\int_{\mathcal{S}} |D(\nabla y|\sqrt{2}b)|$ is the total variation of the vector-valued function $(\nabla y|\sqrt{2}b) : \mathcal{S} \to \mathbb{R}^{3\times 3}$.

Even though we have rigorously derived the thin film limit (5.4) only for energy minimizing deformations, we will use this thin film energy to compute metastable deformations (local minima) by finite element discretization [7]. We consider the case that $\mathcal{S}$ is a polygonal domain and denote by τ a triangulation of $\mathcal{S}$ with its triangular elements denoted by K. The inter-element edges will be denoted by e, and we define the jump of a function ψ across an inter-element edge e separating two elements $K_1, K_2 \in \tau$ by

$$[\![\, \psi \,]\!]_e = \psi_{e,K_1} - \psi_{e,K_2},$$

where ψ_{e,K_i} denotes the trace on e of $\psi|_{K_i}$ for $i = 1, 2$.

For the space of finite element trial functions for the deformation $y(\tilde{x})$ we use $\mathcal{P}_1(\tau)$, the space of continuous functions on $\mathcal{S}$ which are linear on each $K \in \tau$, and for the space of finite element trial functions for the midplane strain $b(\tilde{x})$ we use $\mathcal{P}_0(\tau)$, the space of functions on $\mathcal{S}$ which are constant on each $K \in \tau$. Thus, the space of approximate admissible functions is given by

$$\mathcal{A}_\tau = \mathcal{P}_1(\tau) \times \mathcal{P}_0(\tau) \subset \mathcal{A}.$$

For $(y, b) \in \mathcal{A}_\tau = \mathcal{P}_1(\tau) \times \mathcal{P}_0(\tau)$ and $\theta, \theta_T \in \mathcal{P}_0(\tau)$, the energy (5.4) is well-defined, and we have that

$$\begin{aligned} \kappa \int_{\mathcal{S}} |D(\nabla y|\sqrt{2}b)| + \int_{\mathcal{S}} \phi(\nabla y(\tilde{x})|b(\tilde{x}), \theta(\tilde{x}), \theta_T(\tilde{x}))\, d\tilde{x} \\ = \kappa \sum_{e \subset \mathcal{S}} \Big| [\![(\nabla y|\sqrt{2}b)]\!]_e \Big|\, |e| + \sum_{K \in \tau} \phi\big(\nabla y|b, \theta, \theta_T\big)|_K\, |K|, \end{aligned} \tag{5.5}$$

where $|K|$ is the area of the element K and

$$\Big| [\![(\nabla y|\sqrt{2}b)]\!]_e \Big| = \Big(\big| [\![\nabla y]\!]_e \big|^2 + 2 \big| [\![b]\!]_e \big|^2 \Big)^{1/2}.$$

We note from (5.5) that no numerical integration is required to evaluate the energy $\mathcal{E}(y, b; \theta, \theta_T)$ when $(y, b) \in \mathcal{A}_\tau = \mathcal{P}_1(\tau) \times \mathcal{P}_0(\tau)$ and θ, $\theta_T \in \mathcal{P}_0(\tau)$.

6. Compositional Fluctuation

Assuming that the crystal has an average composition $\bar{c} = |\mathcal{S}|^{-1} \int_{\mathcal{S}} c(\tilde{x})\, d\tilde{x}$ that corresponds to a transformation temperature $\bar{\theta}_T$, we model the spatially varying transformation temperature $\theta_T(\tilde{x})$ by independent normally distributed random variables $\theta_T|_K$, indexed by the triangles $K \in \tau$, with mean $\bar{\theta}_T$ and standard deviation σ. Thus, $\theta_T \in \mathcal{P}_0(\tau)$ is a piecewise constant function with respect to the finite element triangulation, τ, and we obtain a value for $\theta_T|_K$ on each triangle $K \in \tau$ by using a normally distributed pseudo-random number generator with mean $\bar{\theta}_T$ and standard deviation σ.

7. Physical constants

The transformation temperature $\theta_T(\tilde{x})$ is constructed as in Section 6 as independent normally distributed random variables $\theta_T|_K$, indexed by the triangles $K \in \tau$ from the mean transformation temperature $\bar{\theta}_T$ and standard deviation σ

$$\bar{\theta}_T = 270 \text{ K} \quad \text{and} \quad \sigma = 25 \text{ K}. \tag{7.1}$$

The other transformation temperatures are then defined as piecewise constant functions with respect to the triangles K in the triangulation τ by

$$A_f(\tilde{x}) = \theta_T(\tilde{x}) + 5, \qquad M_s(\tilde{x}) = \theta_T(\tilde{x}) - 5, \qquad M_f(\tilde{x}) = \theta_T(\tilde{x}) - 15. \tag{7.2}$$

It follows from (7.1) and (7.2) that $A_f(\tilde{x})$, $M_s(\tilde{x})$, and $M_f(\tilde{x})$ all have standard deviation σ and mean values

$$\bar{A}_f = 275 \text{ K}, \qquad \bar{M}_s = 265 \text{ K}, \qquad \bar{M}_f = 255 \text{ K}.$$

We note that $\theta_T(\tilde{x}) = (M_s(\tilde{x}) + A_f(\tilde{x}))/2$ as proposed in [31].

We present computational results for two sets of lattice constants. For the case $c < a$, we chose the measured lattice constants of $Fe_{70}Pd_{30}$ near its transformation temperture at 270 K [19]

$$a_0 = 3.75 \text{ Å}, \qquad a = 3.81 \text{ Å}, \qquad c = 3.65 \text{ Å},$$

which yield the transformation stretches (2.5)

$$\alpha = \frac{a}{a_0} = 1.016, \qquad \gamma = \frac{c}{a_0} = 0.9733. \tag{7.3}$$

For the case $c > a$, we chose the transformation stretches (2.5)

$$\tilde{\alpha} = \frac{\tilde{a}}{\tilde{a}_0} = 0.9837, \qquad \tilde{\gamma} = \frac{\tilde{c}}{\tilde{a}_0} = 1.0260. \tag{7.4}$$

We set the surface energy parameter $\kappa = 10^{-4}$ GPa $\cdot\, L$ m where L is the physical length of the computational domain which has been scaled to $\mathcal{S} = (0,1) \times (0,1)$. Since the elastic moduli have been taken to be of the order 100 GPa, the dimensionless surface energy $\kappa/(\mathbb{C}L)$ is of the order 10^{-6}.

A surface energy parameter of order 10^{-4} GPa $\cdot\, L$ m was found in [7] to be large enough to have a regularizing effect in numerical simulations of indentation, but smaller values did not have an observable effect. Methods for determining the surface energy parameter κ from experimental data include the analysis of the phonon dispersion curve [20] and the analysis of the length scale of twinning [23].

8. Numerical algorithm for the thermal cycle

We construct our finite element mesh by dividing the square computational domain $\mathcal{S} = (0,1) \times (0,1)$ into $N \times N$ congruent squares with sides of length $h = 1/N$. Each of these squares is further subdivided into four triangles by the diagonals of the square. The results will be presented on meshes with $N = 100$, so there are $4 \cdot 100^2$ triangles $K \in \tau$.

We will present numerical results in Figures 3–5 using our model for the quasi-static cooling of the thin film from 315 K to 215 K and then heating from 215 K to 315 K in increments of 2 K, so we define the temperature sequence

$$\theta_\ell = 315 - 2\ell \qquad \text{for } \ell = 0, \dots, 50, \tag{8.1}$$

$$\theta_\ell = 215 + 2(\ell - 50) \qquad \text{for } \ell = 51, \dots, 100. \tag{8.2}$$

We assume that the rate of cooling and then heating is slow enough so that the film is always in elastic equilibrium at a constant temperature.

We start the simulation with the film at 315 K in a flat austenitic state given by

$$\begin{aligned} y_0(x_1, x_2) &= (x_1, x_2, 0) \quad \text{for all } \tilde{x} = (x_1, x_2) \in \mathcal{S}, \\ b_0(x_1, x_2) &= (0, 0, 1) \quad \text{for all } \tilde{x} = (x_1, x_2) \in \mathcal{S}. \end{aligned} \tag{8.3}$$

The deformation $(y_\ell, b_\ell) \in \mathcal{A}_\tau$ for $\ell = 1, \dots, 100$ is then obtained by computing a local minimum for the energy $\mathcal{E}(y, b; \theta_l, \theta_c)$ by the Polak-Ribière conjugate gradient method [30] with initial iterate

$$(y_\ell^{[0]}, b_\ell^{[0]}) = (y_{\ell-1}, b_{\ell-1}) + (\delta y_\ell, 0), \tag{8.4}$$

where random vibrations are modeled by δy_ℓ. The components of δy_ℓ at the nodes of the triangulation are computed by a normally distributed pseudo-random number generator with mean 0 and standard deviation $0.005h$. We note that since the values of the computed pseudo-random δy_ℓ at the mesh points are independent, the standard deviation of the derivatives of δy_ℓ are $0.005\sqrt{2}$ and $0.005\sqrt{6}$ depending on the orientation of the triangle. If the conjugate gradient iterations have converged to an acceptable tolerance after M iterations, we set

$$(y_\ell, b_\ell) = (y_\ell^{[M]}, b_\ell^{[M]}).$$

The Figures 3–5 show the deformation gradient $(\nabla y|b)|_K$ on each element K. The deformation gradient $(\nabla y|b)|_K$ is exhibited by a coloring scheme whereby the coloring of the element is determined by the distance to the nearest phase or variant [26]. In our coloring scheme, elements near the cubic phase $F \in \mathrm{SO}(3)$ are colored a shade of grey and elements near the tetragonal variants are colored shades of red for $F \in \mathrm{SO}(3)U_1$, shades of yellow for $F \in \mathrm{SO}(3)U_2$, and shades of blue for $F \in \mathrm{SO}(3)U_3$.

9. Numerical results

We present in Figures 3–5 graphical output of our computations for the evolution of the thin film microstructure during the cooling process (8.1) at 285 K, 275 K, 265 K, and 225 K and then the heating process (8.2) at 225 K, 265 K, 275 K, and 285 K.

We first discuss the numerical results in Figure 3 for the evolution of the transformation when the tetragonal lattice constants $c < a$ are given by (7.3) and the tetragonal elastic moduli $\mathbb{C}^M_{11} > \mathbb{C}^M_{33}$ are given by (4.3). The film starts the quasi-static cooling process (8.1) at 315 K in the flat cubic phase (8.3). Since 315 K is $8\sigma/5$ above $\bar{A}_f = 275$ K, the film remains almost uniformly in the cubic phase near 315 K. We see in Figure 3 that at 285 K the film has transformed to the tetragonal phase on a sparse random set of triangular elements $K \in \tau$ since 285 K is $2\sigma/5$ above $\bar{A}_f = 275$ K and $6\sigma/5$ above $\bar{M}_f = 255$ K.

When the film is cooled to 275 K, we see the emergence of tweed-like diagonal oscillations (even though 275 K is still greater than the mean transformation temperature $\bar{\theta}_T = 270$ K) as a consequence of the softening of the cubic elastic modulus $a(\theta)$ in triangular elements $K \in \tau$ for which the softening temperature $M_s(\tilde{x}) = \theta_T(\tilde{x}) - 5$ is close to or greater than 275 K. We note that 275 K is $2\sigma/5$ above $\bar{M}_s = 265$ K and $4\sigma/5$ above $\bar{M}_f = 255$ K. In triangular elements $K \in \tau$ where $a(\theta)$ is small or zero, there exists a low-energy path [12] from the cubic phase ($F \in \mathrm{SO}(3)$) to the tetragonal phase ($F \in \mathrm{SO}(3)U_1 \cup \mathrm{SO}(3)U_2 \cup \mathrm{SO}(3)U_3$), although elastic stresses on $K \in \tau$ from the neighboring triangular elements $\bar{K} \in \tau$ may resist the transformation.

To see this, we consider a path $F : [0,1] \to \mathbb{R}^{3\times 3}_+$ from the cubic phase ($F \in \mathrm{SO}(3)$) such that its right Cauchy-Green strain satisfies $C(s) = F^T(s)F(s) = I + s(\hat{C} - I)$ for some $\hat{C} \in \mathbb{R}^{3\times 3}_+$. At temperatures $\theta \le M_s$, since $\alpha(\theta) = 0$ we have by (3.2) that $W_A(C(s), \theta) = 0$ along the entire path $s \in [0,1]$ if and only if

$$\mathrm{tr}(\hat{C}) = 3 \quad \text{and} \quad \hat{C}_{ij} = 0 \text{ for } i \neq j. \tag{9.1}$$

However, for the transformation stretches (7.3) we have that the right Cauchy-Green strain corresponding to a tetragonal variant $C_\ell = U_\ell^2$ for any $\ell \in \{1,\, 2,\, 3\}$ does not satisfy $\mathrm{tr}(\hat{C}) = 3$, but rather satisfies

$$\mathrm{tr}(C_\ell) = 3.012 \quad \text{and} \quad C_{\ell,ij} = 0 \text{ for } i \neq j. \tag{9.2}$$

Thus, for $\theta \le M_s$ and any $\ell \in \{1,\, 2,\, 3\}$ there is a path $C(s) = I + s(\hat{C} - I)$ close to the path $C(s) = I + s(C_\ell - I)$ such that $W_A(C(s), \theta) = 0$ for $s \in [0,1]$. Now for $\theta \le M_s$ we have that the free energy difference between the cubic and tetragonal phases (2.10) satisfies $\eta(\theta, M_s) < 0$ and the free energy density (2.9) satisfies $\phi(F, \theta, \theta_T) < 0$ in the energy well defined by $W_M(F^TF, \theta) < -\eta(\theta, \theta_T)$. Since the energy well $W_M(F^TF, \theta) < -\eta(\theta, \theta_T)$ does not contain $F \in \mathrm{SO}(3)$ if $\theta > M_f$, we have for $M_f < \theta \le M_s$ that there exists $s_0 > 0$ such that $\phi(F(s), \theta, \theta_T) = W_A(C(s), \theta) = 0$ for $s \in [0, s_0]$ and $\phi(F(s), \theta, \theta_T) = W_M(C(s), \theta) + \eta(\theta, \theta_T) < 0$ for $s \in (s_0, 1]$.

We see from the contour plot in Figure 2 of $\zeta(C_{11}, C_{33}) = \phi(C^{1/2}, M_s, \theta_T)$ for the right Cauchy-Green strain $C = \mathrm{diag}(C_{11}, C_{11}, C_{33})$ with vertical axis $\mathrm{Tr}\, C - 3$ and horizontal axis $C_{11} - C_{33}$ that there is a path from the cubic phase ($C = I$) that has zero energy density and follows the bottom of a horizontal valley until it falls into the energy well of the tetragonal phase ($C = U_3^2$).

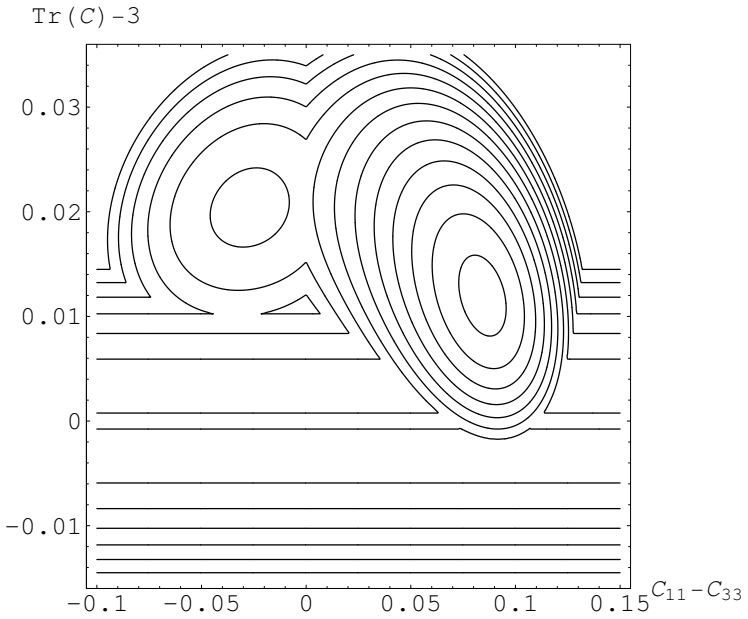

FIGURE 2. Contour plot of $\zeta(C_{11}, C_{33}) = \phi(C^{1/2}, M_s, \theta_T)$ for the right Cauchy-Green strain $C = \operatorname{diag}(C_{11}, C_{11}, C_{33})$ with vertical axis $\operatorname{Tr} C - 3$ and horizontal axis $C_{11} - C_{33}$. The cubic phase ($C = I$) is at $(0, 0)$ and the tetragonal phase $\big(C = U_3^2 = \operatorname{diag}(1.032,\ 1.032,\ 0.947)\big)$ is at $(0.085,\ 0.012)$. At $\theta = M_s$, the tetragonal phase minimizes the free energy density and there is a zero energy path along the bottom of a horizontal valley between a pair of parallel contour lines for $\zeta = 0.00001$ from the cubic phase to the energy well of the tetragonal phase. Level sets are shown for 0.00001 and $\pm 0.0006m$ for $m = 1,\ 2,\ \ldots$. The energy wells corresponding to the martensitic variants $C = U_1^2$ and $C = U_2^2$ have center at $(-0.03,\ 0.02)$ and coincide by symmetry in this projection. The free energy density ϕ was evaluated with tetragonal elastic moduli $\mathbb{C}_{11}^M > \mathbb{C}_{33}^M$ (4.3).

As the film is cooled to 265 K and 225 K, we see that the small tweed-like diagonal oscillations grow in amplitude to become martensitic layered microstructure. As the film is further cooled to 215 K and then heated back to 315 K, we observe at 225 K, 265 K, 275 K, and 285 K that the tetragonal phase transforms back to the cubic phase through tweed-like oscillations. As expected in a first-order phase transformation, we also observe hysteresis as more of the tetragonal phase is present at each temperature during the heating cycle as compared to the cooling cycle.

We observe a slight coarsening of the microstructure as the film evolves from tweed-like oscillations to tetragonal microstructure during cooling. Since the film evolves through a sequence of metastable states (local minima) and the coarser states have less surface energy, the degree of coarsening can be controlled by using simulated annealing optimization at each temperature [20]. We do add random vibrations δy_ℓ at each temperature with mean 0 and standard deviation $0.005h$

during the computations in Figures 3–5, but our algorithm does not seek a global minimum since this process would destroy our exploration of hysteresis.

We next compare in Figure 4 the evolution of the microstructure when the set (4.4) of tetragonal elastic moduli with $\mathbb{C}_{11}^M < \mathbb{C}_{33}^M$ is selected, but the same lattice constants (7.3) with $c < a$ are used as in Figure 3. We observe that the development of tweed-like oscillations and then tetragonal microstructure is delayed during cooling and that the transformation to the cubic phase during heating takes place at lower temperatures when compared to the evolution in Figure 3. We also note that the microstructure is slightly coarser in the computations with $\mathbb{C}_{11}^M < \mathbb{C}_{33}^M$ than for $\mathbb{C}_{11}^M > \mathbb{C}_{33}^M$.

We finally compare in Figure 5 the evolution of the microstructure when the lattice constants (7.4) with $c > a$ are used, but the same tetragonal elastic moduli (4.3) of Figure 3 with $\mathbb{C}_{11}^M > \mathbb{C}_{33}^M$ are used. The evolution of the microstructure during cooling and then heating in Figure 5 appears to be similar to that seen in Figure 3 except that the microstructure is slightly coarser for $c > a$ than $c < a$.

References

[1] R. Abeyaratne and S. Vedantam. A lattice-based model of the kinetics of twin boundary motion. *J. Mech. Phys. Solids*, 51:1675–1700, 2003.

[2] R. Adams. *Sobolev Spaces*. Academic Press, New York, 1975.

[3] J. M. Ball and R. D. James. Fine phase mixtures as minimizers of energy. *Arch. Ration. Mech. Anal.*, 100(1):13–52, 1987.

[4] J. M. Ball and R. D. James. Proposed experimental tests of a theory of fine microstructure and the two-well problem. *Phil. Trans. R. Soc. Lond. A*, 338:389–450, 1992.

[5] K. Bhattacharya and R. D. James. A theory of thin films of martensitic materials with applications to microactuators. *J. Mech. Phys. Solids*, 47(3):531–576, 1999.

[6] K. Bhattacharya and R. V. Kohn. Elastic energy minimization and the recoverable strains of polycrystalline shape-memory materials. *Arch. Ration. Mech. Anal.*, 139:99–180, 1997.

[7] P. Bělík and M. Luskin. A computational model for the indentation and phase transformation of a martensitic thin film. *J. Mech. Phys. Solids*, 50:1789–1815, 2002.

[8] P. Bělík and M. Luskin. A total-variation surface energy model for thin films of martensitic crystals. *Interfaces Free Bound.*, 4:71–88, 2002.

[9] M. A. Carpenter and E. K. H. Salje. Elastic anomalies in minerals due to structural phase transitions. *Eur. J. Mineral.*, 10:693–812, 1998.

[10] P. Ciarlet. *Mathematical Elasticity*, volume 1: Three Dimensional Elasticity. North-Holland, Amsterdam, 1988.

[11] J. Dong, J. Xie, J. Lu, C. Adelmann, C. Palmstrom, J. Cui, Q. Pan, T. Shield, R. James, and S. McKernan. Shape memory and ferromagnetic shape memory effects in single-crystal Ni_2MnGa thin films. *J. Appl. Phys.*, 2004.

[12] W. E, W. Ren, and E. Vanden-Eijnden. Energy landscapes and rare events. In *Proceedings of the International Congress of Mathematicians, ICM 2002, Beijing*, volume III, pages 621–630, 2002.

[13] J. L. Ericksen. Bifurcation and martensitic transformations in Bravais lattices. *J. Elasticity*, 28(1):55–78, 1992.

[14] J. L. Ericksen. Local bifurcation theory for thermoelastic Bravais lattices. In *Microstructure and phase transition*, volume 54 of *IMA Vol. Math. Appl.*, pages 57–84. Springer, New York, 1993.

[15] L. C. Evans and R. F. Gariepy. *Measure Theory and Fine Properties of Functions*. CRC Press, Boca Raton, FL, 1992.

[16] D. Gilbarg and N. S. Trudinger. *Elliptic Partial Differential Equations of Second Order*. Springer-Verlag, New York, 1998.

[17] E. Giusti. *Minimal Surfaces and Functions of Bounded Variation*. Birkhäuser Verlag, Basel-Boston, Mass., 1984.

[18] M. E. Gurtin. *Topics in Finite Elasticity*. SIAM, Philadelphia, 1981.

[19] R. C. Jun. *Martensitic phase transformation and ferromagnetic shape memory effect in Fe-Pd single crystals*. PhD thesis, University of Minnesota, 2001.

[20] S. Kartha, J. A. Krumhansl, J. P. Sethna, and L. K. Wickham. Disorder-driven pretransitional tweed in martensitic transformations. *Phys. Rev. B*, 52:803–822, 1995.

[21] W. Kerr, M. Killough, A. Saxena, P. Swart, and A. Bishop. Role of elastic compatibility in martensitic texture evolution. *Phase Transitions*, 69:247–270, 1999.
[22] D. Kinderlehrer. Twinning in crystals II. In S. Antman, J. Ericksen, D. Kinderlehrer, and I. Müller, editors, *IMA Volumes in Mathematics and Its Applications, vol. 3*, pages 185–212, New York, 1987. Springer-Verlag.
[23] R. Kohn and S. Müller. Surface energy and microstructure in coherent phase transitions. *Commun. Pure Appl. Math.*, 47:405–435, 1994.
[24] M. Kružík and F. Otto. A phenomenological model for hysteresis in polycrystalline shape memory alloys. *Zeit. Angew. Math. Mech.*, to appear.
[25] A. E. H. Love. *A Treatise on the Mathematical Theory of Elasticity*. Cambridge University Press, Cambridge, 1927. reprinted by Dover Publications, New York, 1944.
[26] M. Luskin. On the computation of crystalline microstructure. *Acta Numer.*, 5:191–258, 1996.
[27] M. Luskin. Computational modeling of microstructure. In *Proceedings of the International Congress of Mathematicians, ICM 2002, Beijing*, volume III, pages 707–716, 2002.
[28] S. Muto, R. Oshima, and F. Fujita. Elastic softening and elastic strain energy consideration in the FCC-FCT transformation of Fe-Pd alloys. *Acta Metall. Mater.*, 38(4):685–694, 1990.
[29] S.-C. Ngan and L. Truskinovsky. Thermo-elastic aspects of dynamic nucleation. *J. Mech. Phys. Solids*, 50:1193–1229, 2002.
[30] J. Nocedal and S. Wright. *Numerical Optimization*. Springer-Verlag, 1999.
[31] K. Otsuka and C. M. Wayman. *Shape Memory Materials*. Cambridge University Press, Cambridge, UK, 1998.
[32] M. Pitteri and G. Zanzotto. *Continuum models for twinning and phase transitions in crystals*. Chapman and Hall, London, 1996.
[33] P. Plecháč and T. Roubíček. A visco-elasto-plastic model for phase transformations. *Math. Meth. Appl. Sci.*, 25:1281–1298, 2000.
[34] A. Vainchtein. Dynamics of phase transitions and hysteresis in a viscoelastic Ericksen's bar on an elastic foundation. *J. Elasticity*, 57:243–280, 1999.

Pavel Bělík, Department of Mathematics, University of St. Thomas, 2115 Summit Avenue, St. Paul, MN 55105, U.S.A.
E-mail address: pbelik@stthomas.edu

Mitchell Luskin, School of Mathematics, University of Minnesota, 206 Church Street SE, Minneapolis, MN 55455, U.S.A.
E-mail address: luskin@math.umn.edu

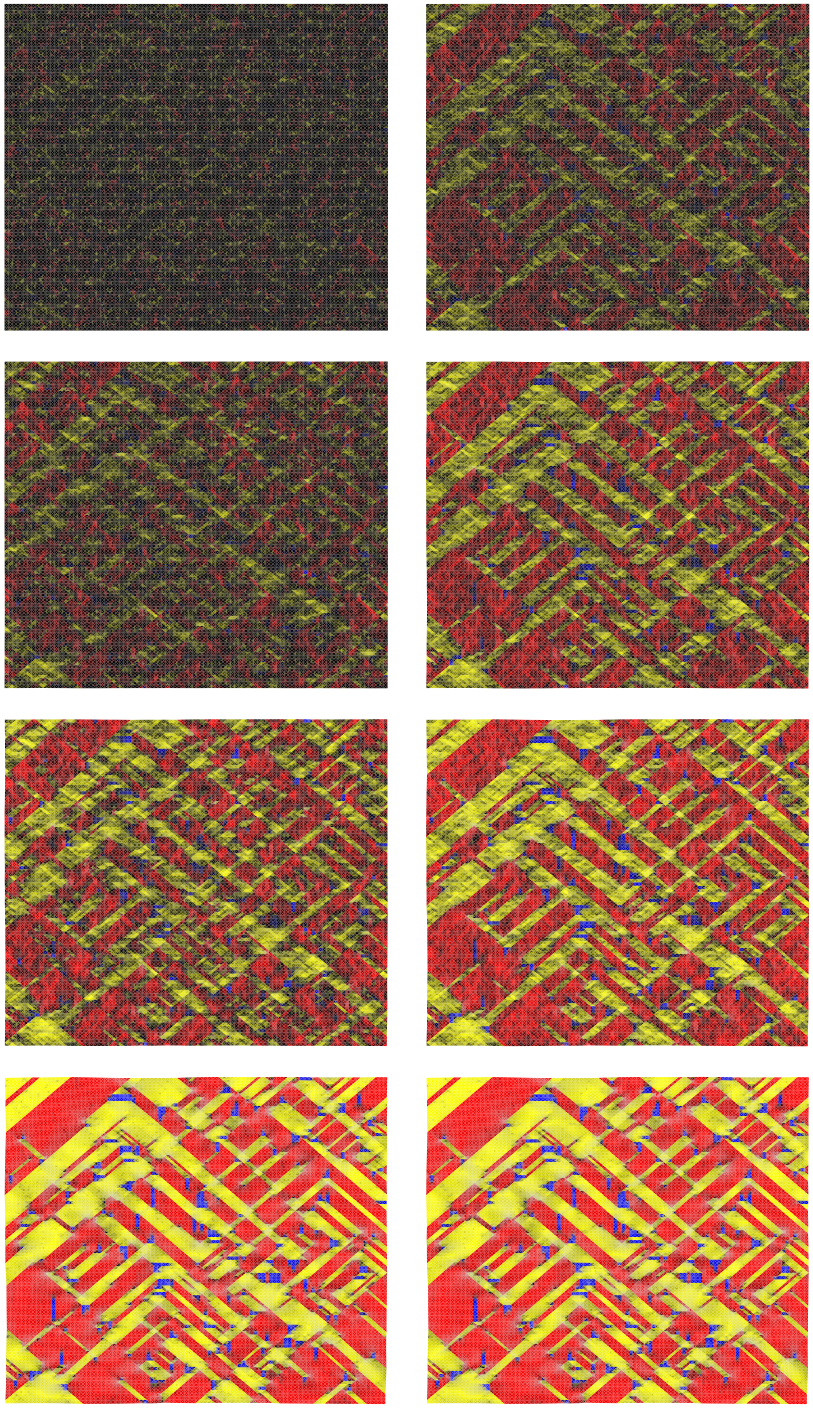

FIGURE 3. Snapshots at 285 K, 275 K, 265 K, and 225 K during cooling (8.1) down the left column and then heating (8.2) up the right column for tetragonal lattice constants $c < a$ (7.3) and tetragonal elastic moduli $\mathbb{C}_{11}^M > \mathbb{C}_{33}^M$ (4.3). The cubic phase is colored gray and the tetragonal variants are colored red, yellow, and blue.

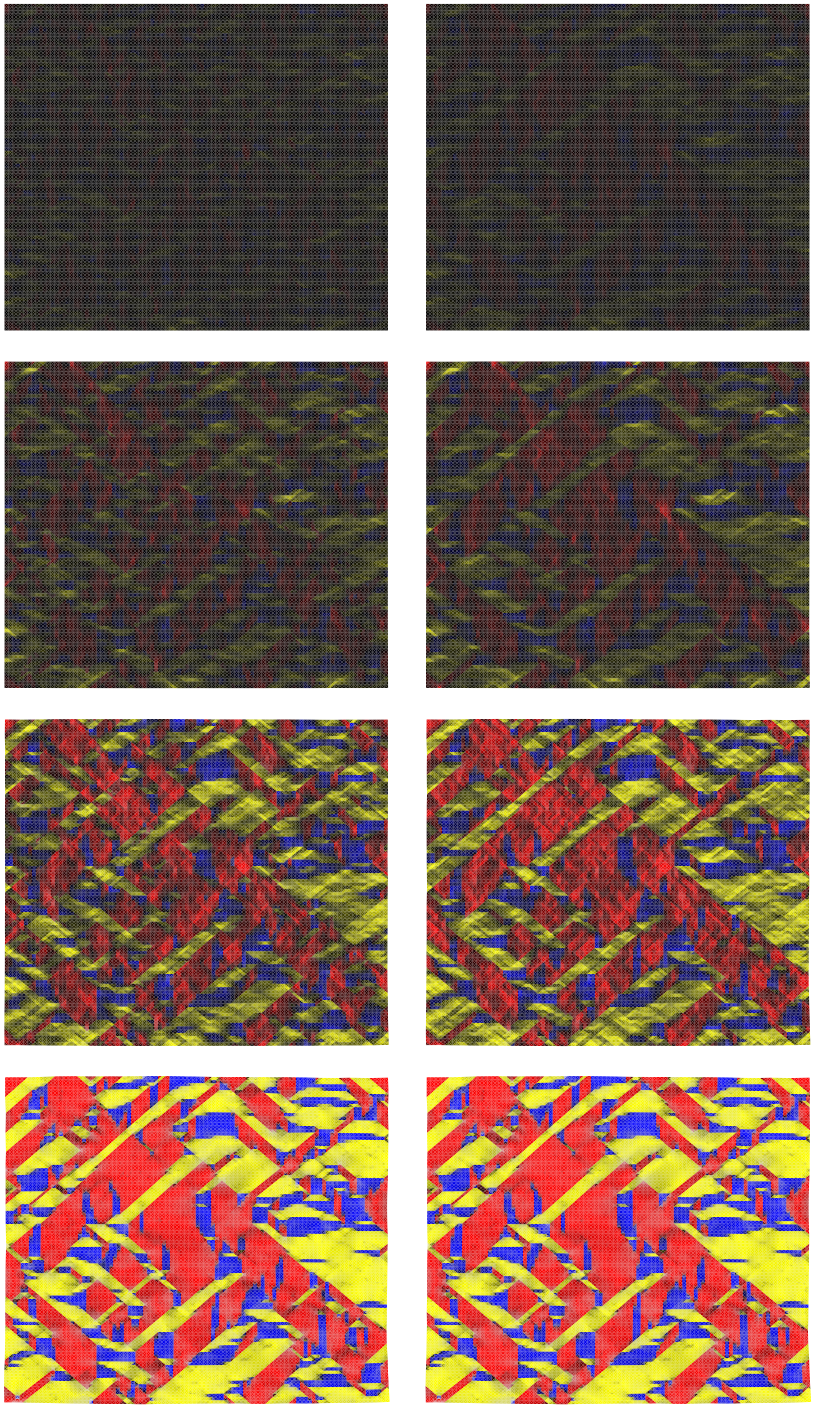

FIGURE 4. Snapshots at 285 K, 275 K, 265 K, and 225 K during cooling (8.1) down the left column and then heating (8.2) up the right column for tetragonal lattice constants $c < a$ (7.3) and tetragonal elastic moduli $\mathbb{C}_{11}^M < \mathbb{C}_{33}^M$ (4.4). The cubic phase is colored gray and the tetragonal variants are colored red, yellow, and blue.

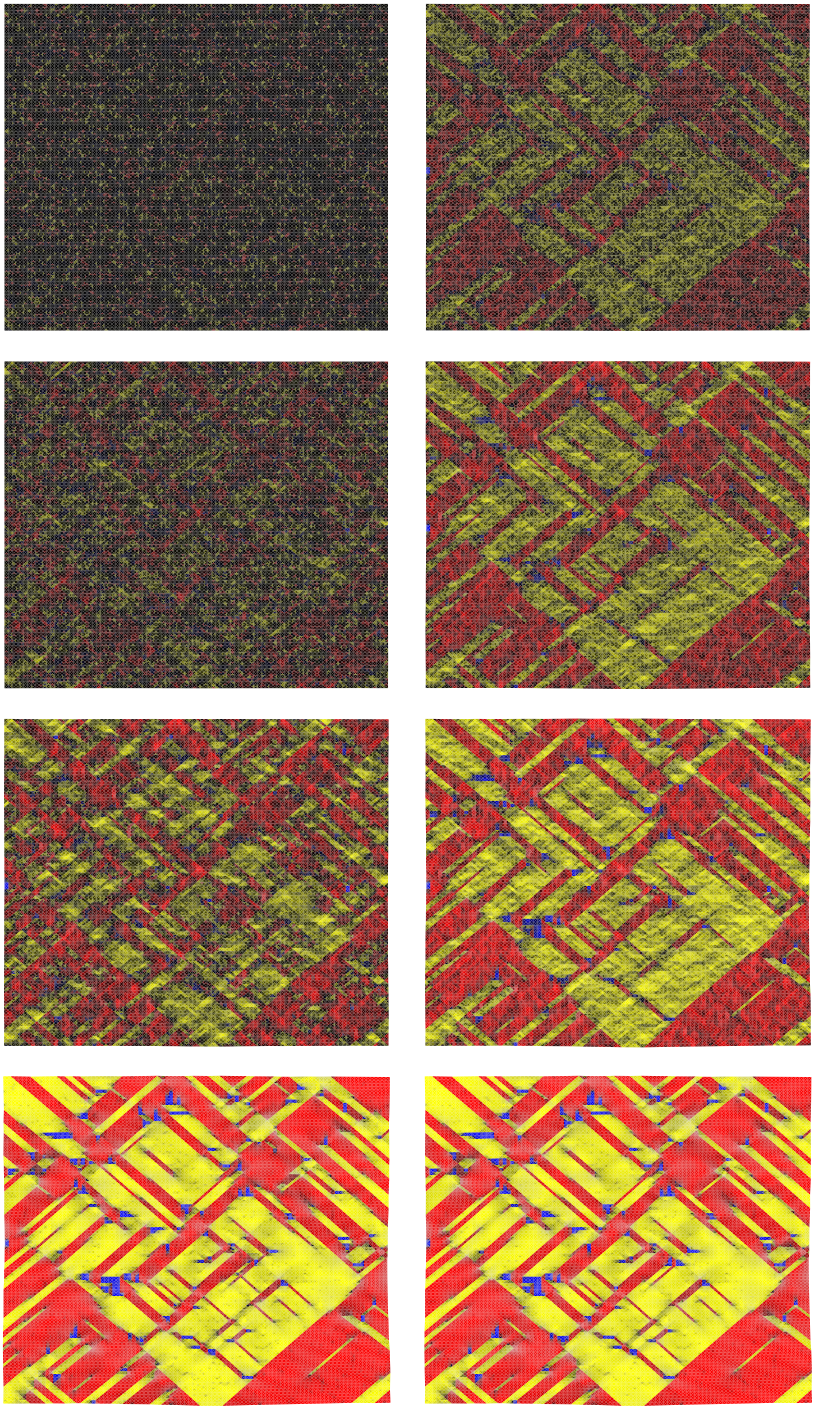

FIGURE 5. Snapshots at 285 K, 275 K, 265 K, and 225 K during cooling (8.1) down the left column and then heating (8.2) up the right column for tetragonal lattice constants $c > a$ (7.4) and tetragonal elastic moduli $\mathbb{C}_{11}^M > \mathbb{C}_{33}^M$ (4.3). The cubic phase is colored gray and the tetragonal variants are colored red, yellow, and blue.